TEKSTİL VE MÜHENDİS

(Journal of Textiles and Engineer)

http://www.tekstilvemuhendis.org.tr

C2C12 HÜCRELERİ KULLANILARAK MİYOKARDİYAL DOKU MÜHENDİSLİĞİ İÇİN ÖRME HAVLU KUMAŞ İSKELENİN IN VITRO DEĞERLENDİRİLMESİ

IN VITRO EVALUATION OF A PILE LOOP KNITTED SCAFFOLD FOR MYOCARDIAL TISSUE ENGINEERING USING C2C12 CELLS

Derya HAROĞLU

Industrial Design Engineering, Engineering Faculty, Erciyes University, Kayseri, Turkey

Online Erişime Açıldığı Tarih (Available online):30 Aralık 2022 (30 December 2022)

Bu makaleye atıf yapmak için (To cite this article):

Derya HAROĞLU (2022): In Vitro Evaluation Of A Pile Loop Knitted Scaffold For Myocardial Tissue Engineering Using C2c12 Cells, Tekstil ve Mühendis, 29: 128, 199-207.

For online version of the article: https://doi.org/10.7216/teksmuh.1221124

TMMOB Tekstil Mühendisleri Odası
UCTEA Chamber of Textile Engineers
Tekstil ve Mühendis
Journal of Textiles and Engineer

Yıl (Year) : 2022/4
Cilt (Vol) : 29
Sayı (No) : 128

Araştırma Makalesi / Research Article

IN VITRO EVALUATION OF A PILE LOOP KNITTED SCAFFOLD FOR MYOCARDIAL TISSUE ENGINEERING USING C2C12 CELLS

Derya HAROĞLU
Industrial Design Engineering, Engineering Faculty, Erciyes University, Kayseri, Turkey

Gönderilme Tarihi / Received: 03.08.2022
Kabul Tarihi / Accepted: 21.11.2022

ABSTRACT: Pile loop knitted scaffold has attracted attention for being used as a three dimensional (3D) biocompatible material particularly for the application of myocardial tissue engineering. In this research, nonintermingled, textured polyethylene terephthalate (PET) multifilament yarn with a filament count of 48 was used for producing a pile loop knit structure to investigate if structure could provide an appropriate microenvironment for the seeded murine C2C12 myoblasts in case of increasing in filament diameter (20.7 micron versus 9.1 micron from the previous study). The resulting structure had a pore network mainly consisting of macropores of 100-200 µm that were well interconnected with micropores (<90 µm). Furthermore, the mean values of the Young's modulus of the structures at 20% strain were 240.67 kPa in the warp direction, and 85.73 kPa in the weft direction, which can be claimed not to be far from those declared in the literature for the human heart muscle. In addition, the cyclic loading-unloading test revealed no creep in the fabric after 100 cycles. According to the results of the WST-1 assay, the 48 filament-based scaffold was non-cytotoxic for C2C12 cells that were able to proliferate properly on the scaffold, which was visualized by SEM and confocal images. In this respect, pile loop knit structures keep promising results for being used as a cardiac patch.

Keywords: Pile loop knitted scaffold, C2C12 myoblasts, myocardial tissue engineering

C2C12 HÜCRELERİ KULLANILARAK MİYOKARDİYAL DOKU MÜHENDİSLİĞİ İÇİN ÖRME HAVLU KUMAŞ İSKELENİN IN VITRO DEĞERLENDİRİLMESİ

ÖZ: Örme havlu kumaş iskele özellikle miyokardiyal doku mühendisliği uygulaması için üç boyutlu (3B) biyouyumlu malzeme olarak dikkat çekmektedir. Bu çalışmada, filament çapının arttırılması durumunda (önceki çalışmadaki 9.1 mikrona karşı 20.7 mikron), yapının, üzerine ekili C2C12 myoblastları için uygun bir mikro çevre sağlayıp sağlamayacağını araştırmak amacıyla, örme havlu bir yapı için 48 filament içeren, puntasız, tekstüre polietilen tereftalat (PET) multifilament iplik kullanıldı. Ortaya çıkan yapı, mikro gözeneklerle (<90 µm) iyi bir şekilde birbirine bağlı olan 100-200 µm aralığındaki makro gözeneklerden oluşan bir gözenek ağına sahip oldu. İlave olarak, yapıların %20 uzamadaki Young's modüllerinin ortalama değerleri çözgü yönünde 240.67 kPa ve atkı yönünde 85.73 kPa olarak bulundu. Bu değerlerin, literatürde bildirilen insan kalp kası değerlerinden çok uzak olmadığı iddia edilebilir. Ayrıca, yorulma testi 100 döngü sonrası kumaşta herhangi bir deformasyon olmadığını gösterdi. WST-1 testi sonuçlarına göre, 48 filament temelli iskele, SEM ve konfokal görüntülerle görselleştirilen, iskele üzerinde düzgün bir şekilde çoğalabilen C2C12 hücreleri için sitotoksik değildi. Bu açıdan, örme havlu yapılar kardiyak yama olarak kullanılmak üzere umut verici sonuçlar vermektedir.

Anahtar Kelimeler: Örme havlu kumaş iskele, C2C12 myoblastları, Miyokardiyal doku mühendisliği

***Sorumlu Yazarlar/Corresponding Author:** dharoglu@erciyes.edu.tr*
***DOI:** https://doi.org/10.7216/teksmuh.1221124 www.tekstilvemuhendis.org.tr*

1. INTRODUCTION

Acute myocardial infarction (AMI), is a potentially fatal coronary heart disease that was claimed to account for approximately nine million people deaths globally in 2017 [1]. An AMI caused by predominantly sudden occlusion of coronary artery, results in irreversible cardiomyocyte loss due to blocking of blood flow, oxygen and nutrients, to the heart muscle [2]. Approximately one billion cardiomyocytes (CMs), nearly one-fourth of the total amount of CMs in the human left ventricule, might be killed very early, in the first hours following AMI [3-5]. Since cardiac regeneration is limited due to the negligible proliferation rate of adult CMs (less than 1% per year), the damaged heart muscle in the infarct-related region is scarred leading to a non-contractile tissue in a few months in survivors [2,6]. Furthermore, lack of synchronous contraction caused by scar tissue impairs the diastolic and systolic function of the heart, inducing cardiac remodeling, ventricular chamber dilatation and wall thinning, favoring death of cells in the surviving CMs months after AMI, ultimately leading to heart failure and death [3,7].

Rapid myocardial reperfusion (<90 min after AMI), pharmacological cardioprotection (e.g., angiotensin-converting enzyme inhibitors), and left ventricular assist devices are today's available therapies; however, none of them could restore lost myocardium [8]. In addition, although heart transplantation is the final therapeutic strategy for end-stage heart failure patients, the application of this option is limited since the number of heart donors is not sufficient (approximately 6,000 heart transplants per year performing globally), and post-transplantation immune complications, risk of tumour formation, and transplant rejection, could potentially develop [6,9].

Cell transplantation therapy has been studied since the early 2000s, with dozens of clinical trials (some of which are continuing), targeting true myocardium regeneration to repair CM loss [10,11]. Here, various cell types such as mesenchymal stem cells, cardiac progenitor cells can either be injected into the damaged myocardium directly through open heart surgery or infused into the infarct-related artery using catheter systems [12]. However, numerous studies have demonstrated that most of the injected cells (>99%) die by less than one week post-implantation [13,14].

Scaffold-based cardiac patch, an anisotropic biocompatible three dimensional (3D) interconnected porous network, which can be used as acellular, or in combination with cells and/or biologically active molecules (e.g., growth factors), has been investigated as an alternative tissue engineering therapeutic approach for a few decades [15,16]. Scaffolds are supposed to improve cell retention on the infarct site by providing a temporary compatible microenvironment with the host myocardium until the seeded cells produce their own extracellular matrix (ECM). Furthermore, scaffolds are required to have mechanical properties close to the native myocardium, where the stiffness is approximately 10-20 kPa at the beginning of diastole (at < 10% strain), and 50 kPa (healthy hearts) - 300 kPa (patients with heart failure) at the end of diastole (at about 15-22% strain) [17,18]. Thus, an optimal scaffold for replacing the injured cardiac muscle with a healthy contractile tissue should support electromechanical integration of CMs to the host myocardium by allowing adequate oxygen and nutrient transfer through a structure with a high surface to volume ratio and correct porosity (>90%), and consequently increasing cell engraftment and survival [19].

To date numerous natural (e.g., collagen, fibrin, alginate, chitosan) or synthetic (e.g., polyurethane, polycaprolactone) biomaterials or their combinations have been used for constructing of scaffolds for both in vitro and in vivo trials. On one hand, natural biomaterials could support cell adhesion, migration, and proliferation, but have batch and source induced variability, and poor mechanical robustness [20,21]. On the other hand, synthetic biomaterials offer good processability, tailorable and proper physical and mechanical properties, but require additional processing to enhance cell adhesion, and the biodegradable ones could have uncontrollable degradation rates and cause inflammation due to acidic degradation products [20,22].

Sridharan et al. [23] produced coaxial polycaprolactone (PCL)-gelatin electrospun fibrous scaffold for culturing and differentiation of human induced pluripotent stem cells (hiPSCs) to cardiomyocytes. They indicated that differentiated cells were migrated and uniformly distributed throughout the developed scaffolds, while they did not observe any difference in the morphology of the hiPSCs in case of culturing on or without scaffolds [23]. Flaig et al. [24] studied poly(lactic acid) (PLA) and PLA:poly(glycerol sebacate) (PGS) nanofibrous scaffolds which were coated with Matrigel and then were seeded with neonatal rat cardiomyocytes. They reported that cardiomyocytes were able to better adhere and spread on PLA:PGS scaffolds in comparison to pure PLA mats [24]. Lin et al. [25] fabricated polyacrylonitrile (PAN) nanofibrous electrospun patches (EP) with random, and aligned orientation to accommodate cardiac anisotropy. They claimed that aligned EP assisted in growth of neonatal rat cardiomyocytes-endothelial cells co-cultivation, and led to a better post-MI ventricular electro-coupling between the patch and the host relative to the randomly oriented EP in case of implantation on a rat heart exposed to experimentally MI [25]. Chen [26] produced rib stitch knitted fabrics from 100% PLA multifilament yarn and PLA/collagen plied yarn as a carrier of cardiosphere derived stem cells (CDCs). It was demonstrated that the PLA/collagen sample gave better results in terms of mechanical properties and cell proliferation in comparison to 100% PLA sample [26].

Textile technology holds promise in tissue engineering and regenerative medicine by mimicking the mechanical, and structural properties of the native tissue to stimulate cell growth through a variety of textile manufacturing techniques including weaving, and knitting. The knitting technique has the ability to provide highly elastic and porous structures, where mechanical properties and porosity can be controlled by changing fiber and yarn parameters, and processing conditions. Furthermore, polyethylene terephthalate (PET) is one of the most used

biomaterials in medical applications including woven vascular grafts, warp-knitted mesh for cardiac support (CorCap™), and composite mesh for hernia repair (Parietex™) as well as cell culture studies [27–29].

The overall goal of this research is to develop a cardiac patch to restore infarcted heart tissue. In the previous study, a pile loop knit fabric made up of 100 denier, intermingled, textured PET yarns that had 144 filaments in cross-section was used as a three dimensional scaffold for the culture of murine C2C12 cells [30]. In this paper, 100 denier, nonintermingled, textured PET multifilament yarn with a filament count of 48 was used for producing a pile loop knit structure to investigate if structure could provide an appropriate microenvironment for the seeded C2C12 cells in case of increasing in filament diameter resulting in change in pore characteristics of fabric. In the previous study, greater proliferation of C2C12 myoblasts on full pile loop knitted fabric could be attributed to the fabric's high surface to volume ratio in comparison to half pile loop knitted fabric (It is referred to as full pile loop when ground and pile loops are knitted together at every round on the machine at full length of the fabric, and half pile loop when pile loops join the formation of knitting structure one in two rounds) [30]. However, not only the high surface to volume ratio but also pore sizes, in other words pore diameters, and the number of large pores in knitted structures could affect C2C12 cell proliferation and viability. Therefore, this study would help design optimal pile loop knitted scaffold and contribute future studies. The physical and mechanical properties including Young's modulus, cyclic loading, morphology, and contact angle of the scaffold were analyzed. The C2C12 cell adhesion and proliferation were evaluated by 2-(4-Iodophenyl)-3-(4-nitrophenyl)-5-(2,4-disulfophenyl)-2H-tetrazolium (WST-1) assay.

2. MATERIALS AND METHODS

In this study, the drawn textured nonintermingled polyethylene terephthalate (PET) yarn was used as a raw material. The PET yarn with the delusterant level of semidull has a filament number of 48 in cross-section. The theoretical number of the PET yarn is 100 denier and all filaments have round cross-sections. The properties of the yarn is given in Table 1.

The filament diameter of the yarn could be measured by ImageJ software from SEM images of filaments, where 10 measurements were done. Breaking strength (g/denier) and breaking elongation (%) of the yarn was tested according to BSENISO2062:2009 [31], Standard Test Method for the Breaking Force and Elongation at Break of Textile Yarns, using a crosshead speed of 250 mm/min and an initial gauge length of 250 mm. The tester was a uniaxial James Heal Titan Strength Tester, the load cell capacity was 1kN, and TestWise™ Software was used to record and analyze the results of five specimens. Crimp contraction, crimp modul, and crimp stability tests were performed according to DIN 53840 (1983) [32] standards by using Textechno Texturmat ME.

One-sided pile loop knit fabric was produced in loose construction, on a circular knitting machine of 20 gauge, 34 inches in diameter, and 1.8 mm pile loop height. After the knitting process, the fabric was washed with water at 60°C for 20 minutes, and then subjected to heat setting at 150 ºC in an industrial machine. In Table 2, the mean values of the physical properties of the knit structure were shown.

Table 1. Properties of the PET yarn

	Measured filament diameter (micron)	Measured linear density (BSENISO2060) (denier)	Tenacity (BSENISO2062) (g/denier)	Elongation (BSENISO2062) (%)	
Mean	20.7	102	4.45	27.35	
SD	1.3	0.13	0.28	2.15	
	Crimp Contraction (CC) (DIN 53840) (%)	Crimp Modul (CM) (DIN 53840) (%)	Crimp Stability (CS) (DIN 53840) (%)	Shrinkage (DIN 53840) (%)	Oil Content (Extraction Method) (%)
Mean	16.35	12.77	70.71	3.22	2.2
SD	0.053	1.62	0.76	0.061	<1

Note: SD: Standard Deviation

Table 2. Dimensional properties of the fabric

Loop length (cm)		Fabric thickness (mm)	Areal density (g/m^2)	Porosity (%)	Air permeability ($cm^3/(cm^2/s)$)	Linear dimensions	
l_g	l_p					wales/cm (w/cm)	courses/cm (c/cm)
0.425	0.739	1.34	133	92.8	177.90	9.3	10.6

The loop lengths of ground (l_g) and pile (l_p) yarns were found by unraveling more than 50 courses, where each course included 50 wales, and the length of yarn was measured in cm [33,34]. When the yarn length was divided by 50, the length of one loop was calculated, and the average loop lengths were recorded from ten specimens [33,34]. The thickness was measured according to the ASTM D1777-96 (2019) [35], Standard Test Method for Thickness of Soft Materials, using CSI® Custom Scientific Instruments, Inc., CSI-55, fabric thickness tester. The values of ten specimens were recorded with a pressure of 2.18 g/cm^2. The areal density (g/m^2) was measured with a conventional circular cutter die with a surface area of 100 cm^2 according to the BS EN 12127 (1998) [36], where five measurements were done. The percentage porosity was calculated by measuring five specimens, and using Equation (1):

$$\text{Porosity} = (1 - \rho/\rho_0) \times 100 \quad (1)$$

where ρ and ρ_0 are the density of the knitted scaffold and the density of the PET polymer (1.38 g/cm^3), respectively. The density of the knitted scaffold was calculated by cutting the scaffold into 1 cm x 1 cm slices (in total five slices) and then weighing the slices on an electronic balance. The air permeability was tested according to the ASTM D737 (2018) [37] using TEXTEST FX 3300 air permeability tester. The testing area was 38 cm^2, and a 125 Pa air pressure was applied during the test. Five specimens were measured, and the test results were recorded in cm^3/(cm^2/s). The number of stitches per unit length (courses/cm) and unit width (wales/cm) were measured on the ground side of the fabric, where ten specimens were considered. All of the measurements were done from the middle part of the fabric to minimize the variability.

This research is made up of three parts. In the first part, uniaxial tensile test, and cyclic loading test in both directions of wales (warp) and courses (weft), pore network analysis, and contact angle tests were carried out. In the second part, the C2C12 cell adhesion and proliferation were evaluated by 2-(4-Iodophenyl)-3-(4-nitrophenyl)-5-(2,4-disulfophenyl)-2H-tetrazolium (WST-1) assay. In the third part, the results were discussed.

2.1. Uniaxial tensile, and cyclic loading test

The uniaxial tensile test of the pile loop knit fabric was done according to ASTM D 5035-11 (2019) [38], Standard Test Method for the Breaking Force and Elongation of Textile Fabrics, utilizing a crosshead speed of 10 mm/min, and an initial gauge length of 25 mm. Specimens were prepared by cutting the knitted fabrics to a length of 90 mm to be long enough to be clamped in the top and bottom jaws, and the width of the specimens was 25 mm.

Young's modulus (E) at 20% strain was calculated considering both engineering and true stress-strain values by using the following equations:

$$E_{eng} = \left(\frac{\sigma eng}{\varepsilon eng}\right)/1000 = \left(\frac{\frac{F}{A0}}{\varepsilon eng}\right)/1000 \quad (2)$$

$$E_{true} = \left(\frac{\sigma true}{\varepsilon true}\right)/1000 = \left(\frac{\frac{F}{A0}}{\varepsilon true}\right)/1000 \quad (3)$$

$$\varepsilon_{true} = \ln(1 + \varepsilon_{eng}) \quad (4)$$

$$\sigma_{true} = \sigma_{eng}(1 + \varepsilon_{eng}) \quad (5)$$

E_{eng}, E_{true}: Young's modulus (kPa)
F: Tensile force applied on the sample (N)
A_0: Initial cross-sectional area of the sample (m^2)
ε_{eng}: Engineering strain
ε_{true}: True strain
σ_{eng}: Engineering stress (kPa)
σ_{true}: True stress (kPa)

The tester was a uniaxial James Heal Titan Strength Tester, the load cell capacity was 1kN, and TestWise™ Software was used to record and analyze the results. Five specimens in each direction (warp and weft) were tested.

The cyclic loading-unloading test (gauge length = 25 mm, speed = 10 mm/min) was conducted by stretching the fabrics to 20% strain, and then releasing them back to strain of 0%, which was repeated for 100 cycles in a dry state at room temperature with the James Heal Titan Strength Tester (n=3). The cyclic lost energy (in the form of heat), an energy loss in a hysteresis loop (Δw), was calculated as follows [39]:

$$\Delta w = \int_0^{\varepsilon} \sigma_{loading} - \sigma_{unloading}\, d\varepsilon \quad (6)$$

2.2. The measurement of knitted fabric morphology

Five scanning electron microscopy (SEM) images of each side, front (surface), and back side (Figure 1 (a), (b)), of the fabric sample were used for analyzing the pore diameters, and pore areas in polygonal shapes surrounded by filaments at different positions of the fabric via the trial version of Digimizer software, image analysis program. The distance between the two adjacent filaments (Figure 1 (a)) was considered as a pore diameter [40].

2.3. Contact angle measurements

Contact angle measurements were performed via the sessile drop method with 4 µl distilled water on a Theta Lite Optical Goniometer (KSV Instruments Ltd, Finland) to determine the wetting property of the knitted structure. Measurements were carried out after the water droplet came into contact with the surface of the fabric's back side for 10 seconds. The average of three different measurements were recorded.

2.4. Biological sample preparation

Knitted fabric sample was cut into 28 mm^2 circular slices and sterilized by autoclave. The scaffold specimens were placed in a non-treated polystyrene 96-well plates (Corning, USA) for the biological experiments. Fibronectin coating solution which was performed by using 10 µg/ml fibronectin (Sigma-Aldrich, USA) solution in 1 ml Fetal Bovine Serum (FBS)-free cell culture media, was added onto the scaffolds for 4 h. Then, all the media and fibronectin solution were aspirated and washed by phosphate-buffered saline (PBS, Biological Industries, USA) for three times.

2.5. Myoblast culture on scaffolds

5 x 10^4 C2C12 mouse myoblast cells (ATCC® CRL-1772™) were seeded onto the specimens in each group (day 3 and day 7). Cell culture media contained Dulbecco's Modified Eagle's Medium (DMEM, Sigma, USA; with 4500 mg/L glucose) supplemented with 10% FBS (Biological Industries, USA).

2.6. Cell viability by WST-1 assay

For WST-1 test, a total of ten specimens were prepared, in which five specimens were used for day 3 of the WST-1 assay, and five for day 7 of the WST-1 assay. After 70 hours for the group of day 3, and after 166 hours for the group of day 7, cell proliferation reagent WST-1 (Takara, MK400) solution was added to each well at 10% of the well volume. Then, the culture plate was incubated for 2 hours in a 37ºC humidified CO_2 incubator. The absorbance values were read at a test wavelength of 450 nm (A450) and a reference wavelength of 630 nm (A630) (Chromate 4300 Elisa Reader, USA). The percentage of cell viability was calculated as follows [41]:

where blank represents well with DMEM medium containing 10% FBS, without any cell; and, positive control means well including cells cultured in DMEM supplemented with 10% FBS, without any scaffold; considered as 100% viable. Furthermore, negative control (cytotoxicity control) was designated by treating cultured cells with hydrogen peroxide (H_2O_2) known as the most stable reactive oxygen species (ROS), at the concentration of 2% for 24 hours at day 2 for the group of day 3, and at day 6 for the group of day 7, without any scaffold.

2.7. Cell attachment by scanning electron microscopy (SEM) and confocal microscopy

For SEM imaging, first, most of the culture media was removed, then, the cells were fixed using a fixative containing 4% glutaraldehyde (EMS, 16210) for 1 hour at 4ºC. Second, the specimens were washed three times with 500 µl PBS for 5 minutes each. Third, all the specimens were dehydrated through a series of ethanol concentrations (30, 50, 70, 90, 95, and 100%). Fourth, critical point drying was conducted by a critical point dryer (Leica EM CPD300). Fifth, the specimens were sputter coated with gold/palladium in a Leica EM ACE 600 sputter coater. The prepared PET scaffold specimens were then viewed in a Hitachi Regulus 8230 scanning electron microscope. For confocal imaging, after the removal of the culture media, each cell seeded scaffold specimen was treated with 100 µl NucBlue™ (DAPI: 4',6-diamidino-2-phenylindole) live staining dye (Invitrogen), and then incubated for 30 minutes. The specimens were observed using a Zeiss LSM 800 confocal microscope.

2.8. Statistical analysis

The one way analysis of variance (ANOVA) was used for statistical anaysis by utilizing the trial version of JMP® 16 statistical software. *p*-values smaller than 0.05 were considered significant.

3. RESULTS AND DISCUSSION

3.1. The morphology of knit structure

Figure 1 shows the morphology of the knitted structure.

$$\text{Cell Viability (\%)} = \frac{[A450\,(Sample) - A630\,(Sample)] - [A450\,(Blank) - A630\,(Blank)]}{[A450\,(Positive\ Control) - A630\,(Positive\ Control)] - [A450\,(Blank) - A630\,(Blank)]} * 100 \qquad (7)$$

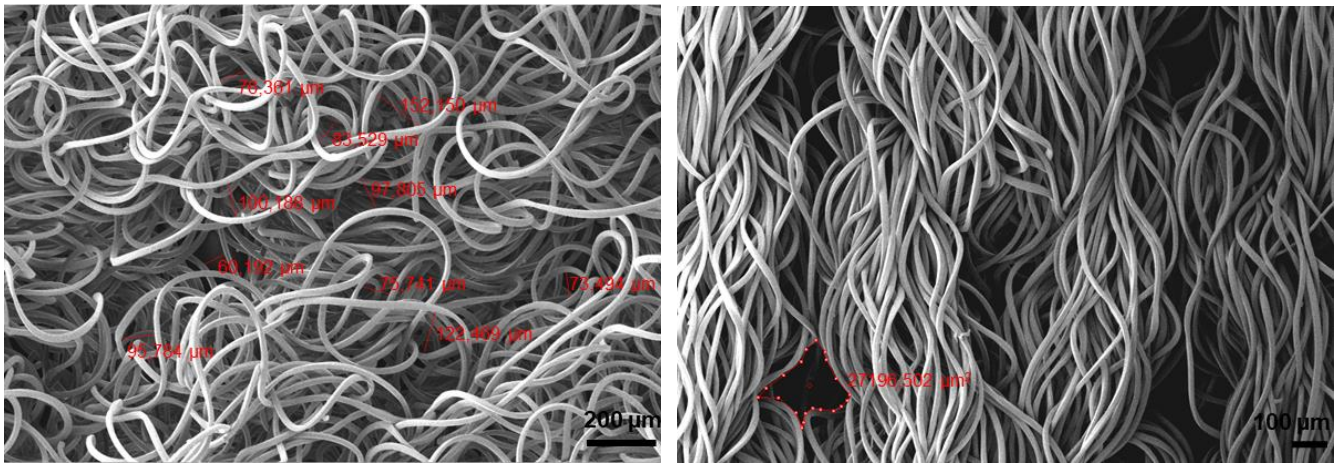

(a) (b)

Figure 1. Knitted structure (a) surface morphology, (b) back side morphology

Few pores in polygonal shapes were observed just on the back side of the fabric, but not on the front side unlike the fabrics made up of textured PET yarns that had 144 filaments in cross-section [30,42]. The structure was recognized to provide a pore network mainly consisting of macropores of 100-200 µm that were well interconnected with micropores (<90 µm) as shown in Figure 2. The outliers marked as dots in Figure 2 belong to the diameters of pores in polygonal shapes. Furthermore. the mean pore area in polygonal shapes was measured as 25147.09 µm^2 (n=5).

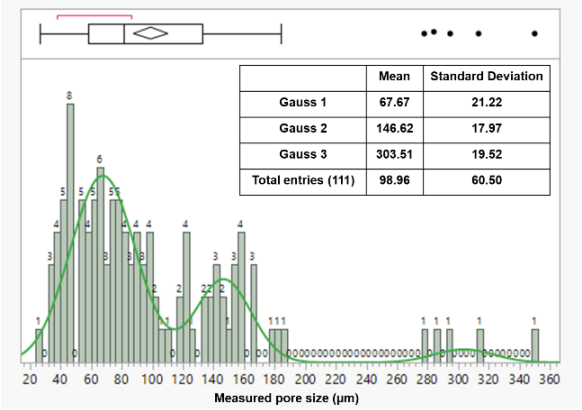

Figure 2. Histograms of pore diameter distribution of the knitted scaffold

3.2. The wettability property of knit structure

An increase in the contact angle, the angle between the liquid droplet and the solid surface, decreases the liquid wetting of the surface [43].

According to the current literature, the factors affecting the wettability properties of pile loop knit structures can be claimed to include filament count and diameter, pore characteristics (e.g., pore sizes, number of pores) of the fabric, surface roughness, and areal density.

The contact angle of the knitted structure, of which microscopic view is shown in Figure 3, was measured as 140º (standard deviation (sd): 4.68). Although the porous nature and mechanical properties of pile loop knit structures made up of PET yarns make them ideal candidates for cardiac tissue engineering their hydrophobic surface does not offer a favorable microenvironment for cell adhesion and proliferation [44]. Thus, scaffolds with hydrophobic nature can preferably be coated with ECM proteins (e.g., fibronectin, collagen type I) to promote cell attachment and migration [45].

Figure 3. Microscopic view of the structure

The high contact angle can be explained by the low air permeability value of the structure, in other words, few macropores per unit area in the fabric. Here, the diameters of 100–200 µm and less than 90 µm, correspond to macropore and micropore, respectively, by considering the morphology section of the paper.

3.3. Stress-strain curves, Young's modulus and cyclic loading

Figure 4 (a) and (b) shows the stress-strain and cyclic loading and unloading curves of the knitted scaffold in the direction of wales and courses, respectively.

In the stress-strain curves, the portions up to 20% strain are in the elastic region of the fabric, where for the linear regions, the coefficient of regression (RSquare) is approximately 98% both in the direction of warp and weft.

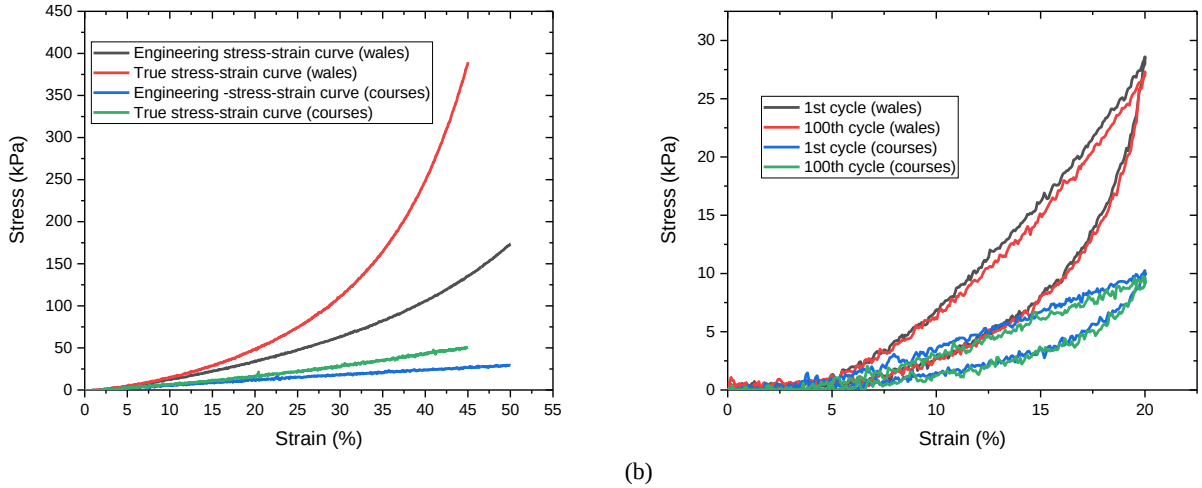

(a) (b)

Figure 4. (a) Stress-strain curves of the knitted scaffold (b) Cyclic loading-unloading curves of the knitted scaffold on the basis of engineering stress and strain values.

The values of the Young's modulus of the structure at 20% strain in the warp and weft directions were calculated by using both engineering and true stress-strain curves, which are shown in Table 3.

It can be seen from the Figure 4 (b) that the hysteresis loops are not displaced along the X-axis both for the direction of warp and weft, signifying no creep in the material.

The cyclic energy loss (Δw), the area inside the hysteresis loop, decreased slightly with the increase in number of cycles both in warp and weft directions (Figure 5), which can be attributed to molecular reorientation of polymer chains under cyclic loading, indicative of the first stages of a fatigue test [46,47].

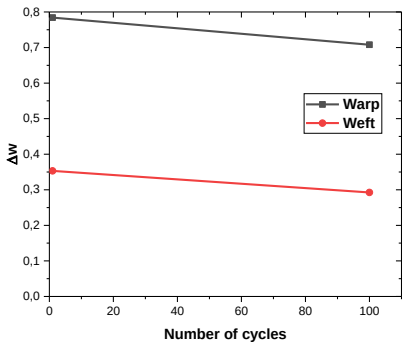

Figure 5. Variation of cyclic energy loss of knitted structure in warp and weft directions with the number of cycles

3.4. Cell viability by WST-1 assay

WST-1 assay demonstrated proper viability of C2C12 myoblasts on the scaffold (Figure 6). The mean cell viability value increased from 121.22% (sd: 3.63) on day 3 to 171.53% (sd: 7.76) on day 7, where the difeerence between the values on day 3 and day 7 was statistically important (p-value < 0.05). The mean cell viability of the negative control was 13.92% (sd: 1.25) both on day 3 and on day 7, where H_2O_2 had a significant cytotoxic effect in C2C12 cells [48].

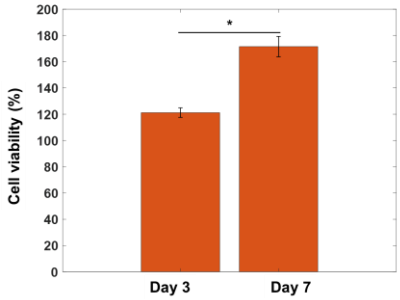

Figure 6. In vitro test of cell viability (%) on day 3 and day 7

The SEM image revealed that the cells attached and grew along the surface of the PET filament (Figure 7 (a)), and confocal microscopy analysis visualized the presence of C2C12 cells on the scaffold, supporting the cell viability results (Figure 7 (b)).

Table 3. Young's modulus of knitted scaffold

	E_{eng} (kPa) at 20% strain		E_{true} (kPa) at 20% strain	
	Warp direction	Weft direction	Warp direction	Weft direction
Mean	162.19	60.91	240.67	85.73
SD	8.92	5.01	11.16	8.81

Note: SD: Standard Deviation

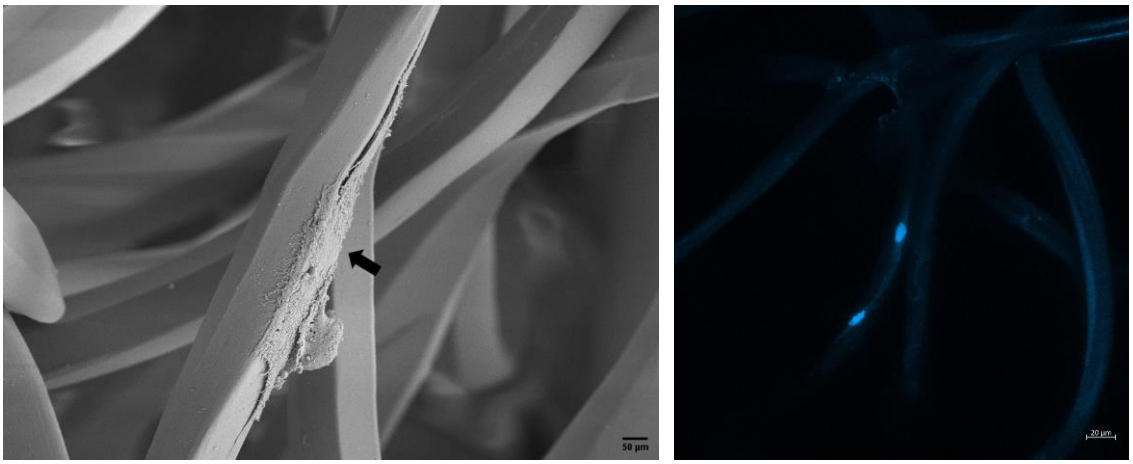

(a) (b)

Figure 7. SEM and confocal microscopy imaging (a) SEM image of C2C12 cell attached to PET filament, 1500X (b) Confocal microscopy image of C2C12 cells on knitted scaffold stained with DAPI (blue)

Although there are many researches [49–51] as to how fiber diameter and porosity guide cell response, proliferation, and migration, the use of different cell types from different species, different structures (e.g., electrospun mat, additive manufacturing), and different culture media complicates the comparison.

This study demonstrated that an approximately 128% increase (20.7 micron versus 9.1 micron [30]) in the diamater of filaments, leading to a structure with a different pore network, did not adversely influence C2C12 cell viability on the scaffold. Furthermore, since the structure can provide control over the fiber diameter and porosity, the outcomes of the study would contribute to the design of ideal pile loop knitted scaffolds particularly for application of myocardial tissue engineering.

4. CONCLUSION

In this paper, the physical and mechanical properties (e.g., morphology, wettability, Young's modulus, cyclic loading) of the pile loop knit fabric made up of 100 denier textured PET yarns with a filament number of 48 in cross-section were analyzed for the purpose of being used as a scaffold for myocardial tissue engineering. An approximately 128% increase (20.7 micron versus 9.1 micron from the previous study [30]) in the diamater of filaments resulted in a structure with a pore network mainly consisting of macropores of 100-200 μm that were well interconnected with micropores (<90 μm). Furthermore, the mean values of the Young's modulus of the samples at 20% strain were 240.67 kPa in the warp direction, and 85.73 kPa in the weft direction, on the basis of the results of the true stress-strain curves. Here, the values of the Young's modulus can be claimed not to be far from the announced values (50 kPa (healthy hearts) - 300 kPa (patients with heart failure) at about 15-22% strain) [17,18]. In addition, the cyclic loading-unloading test revealed no creep in the fabric after 100 cycles.

The pile loop knitted scaffold was seeded with C2C12 cells, and the cell proliferation and viability were evaluated by WST-1 assay. The results of the WST-1 assay showed that murine C2C12 myoblasts proliferated conveniently on the 48 filament-based scaffold. The scaffold was non-cytotoxic for C2C12 cells that were able to attach and grow along the surface of the PET filament, which was visualized by SEM and confocal images.

To sum up, pile loop knit structures keep promising results for being used as a cardiac patch. The outcomes of this research would contribute to future studies in terms of developing ideal scaffolds especially for applications of myocardial tissue engineering.

ACKNOWLEDGEMENTS

The author is thankful to the administration of Boyteks, Erciyes Anadolu Holding A.S., and University of Eskisehir Osmangazi Central Research Laboratory Application and Research Center for their support during the research work.

REFERENCES

1. Dai, H., Much, A. A., Maor, E., Asher, E., Younis, A., Xu, Y., Lu, Y., Liu, X., Shu, J., Bragazzi, N. L. (2022), *Global, regional, and national burden of ischaemic heart disease and its attributable risk factors, 1990–2017: results from the Global Burden of Disease Study 2017*, European Heart Journal-Quality of Care and Clinical Outcomes, 8(1), 50–60.
2. Mechanic, O. J., Gavin, M., Grossman, S. A., Ziegler, K., (2021), *Acute Myocardial Infarction (Nursing)*, StatPearls, Treasure Island (FL): StatPearls Publishing.
3. Abbate, A., Bussani, R., Amin, M. S., Vetrovec, G. W., Baldi, A., (2006), *Acute myocardial infarction and heart failure: Role of apoptosis*, International Journal of Biochemistry & Cell Biology, 38(11), 1834–1840.
4. Murry, C. E., Reinecke, H., Pabon, L. M., (2006), *Regeneration Gaps: Observations on Stem Cells and Cardiac Repair*, Journal of the American College of Cardiology, 47(9), 1777–1785.
5. Laflamme, M. A., Murry, C. E., (2011), *Heart regeneration*, Nature, 473(7347), 326–335.
6. Bar, A., Cohen, S., (2020), *Inducing Endogenous Cardiac Regeneration: Can Biomaterials Connect the Dots?*, Frontiers in Bioengineering and Biotechnology, 8, 126.
7. Portillo Esquivel, L. E., Zhang, B., (2021), *Application of Cell, Tissue, and Biomaterial Delivery in Cardiac Regenerative Therapy*, ACS Biomaterials Science & Engineering, 7(3), 1000–1021.
8. Heusch, G., (2020), *Myocardial ischaemia–reperfusion injury and cardioprotection in perspective*, Nature Reviews Cardiology, 17(12), 773–789.
9. Khush, K. K., Potena, L., Cherikh, W. S., Chambers, D. C., Harhay, M. O., Hayes, D., Hsich, E., Sadavarte, A., Singh, T. P., Zuckermann, A., Stehlik, J., (2021), *The International Thoracic Organ Transplant Registry of the International Society for Heart and Lung Transplantation: 37th adult heart transplantation report—2020; focus on deceased donor characteristics*, Journal of Heart and Lung Transplantation, 39(10), 1003–1015.
10. MacArthur, J. W., Goldstone, A. B., Cohen, J. E., Hiesinger, W., Woo, Y. J., (2016), *Cell transplantation in heart failure: where do we stand in 2016?*, European Journal of Cardio-Thoracic Surgery, 50(3), 396–399.
11. Bolli, R., (2020), *Cell therapy for acute myocardial infarction: Requiescat in Pace*, European Heart Journal, 41(38), 3711–3714.
12. Dib, N., Khawaja, H., Varner, S., McCarthy, M., Campbell, A., (2011), *Cell Therapy for Cardiovascular Disease: A Comparison of Methods of Delivery*, Journal of Cardiovascular Translational Research, 4(2), 177.
13. Vagnozzi, R. J., Sargent, M. A., Molkentin, J. D., (2020), *Cardiac Cell Therapy Rejuvenates the Infarcted Rodent Heart via Direct Injection but Not by Vascular Infusion*, Circulation, 141, 1037–1039.
14. De Pieri, A., Rochev, Y., Zeugolis, D. I., (2021), *Scaffold-free cell-based tissue engineering therapies: advances, shortfalls and forecast*, Nature NPJ Regenerative Medicine, 6(1), 1–15.
15. Rane, A. A., Christman, K. L., (2011), *Biomaterials for the Treatment of Myocardial Infarction: A 5-Year Update*, Journal of the American College of Cardiology, 58(25), 2615–2629.
16. Taylor, D. A., Chandler, A. M., Gobin, A. S., Sampaio, L. C., (2017), *Maximizing Cardiac Repair: Should We Focus on the Cells or on the Matrix?*, Circulation Research, 120(1), 30–32.
17. Reis, L. A., Chiu, L. L. Y., Feric, N., Fu, L., Radisic, M., (2016), *Biomaterials in myocardial tissue engineering*, Journal of Tissue Engineering and Regenerative Medicine, 10(1), 11–28.
18. Chen, Q. Z., Bismarck, A., Hansen, U., Junaid, S., Tran, M. Q., Harding, S. E., Ali, N. N., Boccaccini, A. R., (2008), *Characterisation of a soft elastomer poly(glycerol sebacate) designed to match the mechanical properties of myocardial tissue*, Biomaterials, 29(1), 47–57.

19. Chang, T., Liu, C., Lu, K., Wu, Y., Xu, M., Yu, Q., Shen, Z., Jiang, T., Zhang, Y., (2021), *Biomaterials based cardiac patches for the treatment of myocardial infarction*, Journal of Materials Science & Technology, 94, 77–89.
20. Sharma, S., Srivastava, D., Grover, S., Sharma, V., (2014), *Biomaterials in Tooth Tissue Engineering: A Review*, Journal of Clinical and Diagnostic Research, 8(1), 309.
21. Mei, X., Cheng, K., (2020), *Recent Development in Therapeutic Cardiac Patches*, Frontiers in Cardiovascular Medicine, 7, 294.
22. Chen, Q. Z., Harding, S. E., Ali, N. N., Lyon, A. R., Boccaccini, A. R., (2008), *Biomaterials in cardiac tissue engineering: Ten years of research survey*, Materials Science and Engineering R: Reports, 59(1–6), 1–37.
23. Sridharan, D., Palaniappan, A., Blackstone, B. N., Dougherty, J. A., Kumar, N., Seshagiri, P. B., Sayed, N., Powell, H. M., Khan, M., (2021), *In situ differentiation of human-induced pluripotent stem cells into functional cardiomyocytes on a coaxial PCL-gelatin nanofibrous scaffold*, Materials Science and Engineering: C, 118, 111354.
24. Flaig, F., Ragot, H., Simon, A., Revet, G., Kitsara, M., Kitasato, L., Hébraud, A., Agbulut, O., Schlatter, G. (2020), *Design of Functional Electrospun Scaffolds Based on Poly(glycerol sebacate) Elastomer and Poly(lactic acid) for Cardiac Tissue Engineering*, ACS Biomaterials Science and Engineering, 6(4), 2388–2400.
25. Lin, Y. D., Ko, M. C., Wu, S. T., Li, S. F., Hu, J. F., Lai, Y. J., Harn, H. I. C., Laio, I. C., Yeh, M. L., Yeh, H. I., Tang, M. J., Chang, K. C., Su, F. C., Wei, E. I. H., Lee, S. T., Chen, J. H., Hoffman, A. S., Wu, W. T., Hsieh, P. C. H., (2014), *A nanopatterned cell-seeded cardiac patch prevents electro-uncoupling and improves the therapeutic efficacy of cardiac repair*, Biomaterials Science, 2(4), 567–580.
26. Chen, J., (2020), *Preclinical Evaluation of a Biodegradable Knitted Heart Cap for the Delivery of Cardiosphere-Derived Cells to Induce Reverse Remodeling of a Failing Left*, Thesis, NCSU, USA.
27. Deeken, C. R., Faucher, K. M., Matthews, B. D., (2012), *A review of the composition, characteristics, and effectiveness of barrier mesh prostheses utilized for laparoscopic ventral hernia repair*, Surgical Endoscopy, 26(2), 566–575.
28. Walsh, R. G., (2005), *Design and features of the Acorn CorCap™ Cardiac Support Device: The concept of passive mechanical diastolic support*, Heart Failure Reviews, 10(2), 101–107.
29. Pekkanen-Mattila, M., Hakli, M., Pölönen, R. P., Mansikkala, T., Junnila, A., Talvitie, E., Koivisto, J. T., Kellomaki, M., Aalto-Setala, K., (2019), *Polyethylene terephthalate textiles enhance the structural maturation of human induced pluripotent stem cell-derived cardiomyocytes*, Materials, 12(11), 1805.
30. Haroglu, D., Eken, A., Gonen, Z. B., Bahar, D., (2021), *Development of a three dimensional (3D) knitted scaffold for myocardial tissue engineering. Part II: biological performance of the knitted scaffolds*, The Journal of The Textile Institute, 113(5), 895-905.
31. ISO 2062:2009, *Textiles, Yarns from packages, Determination of single-end breaking force and elongation at break using constant rate of extension (CRE) tester*, International Organization for Standardization, https://www.iso.org/standard/45642.html, accessed Aug. 01, 2022.
32. DIN 53840-1, *Testing of textiles; determination of parameters for the crimp of textured filament yarns; filament yarns with a linear density of up to 500 dtex*, DIN, https://www.din.de/en, accessed Aug. 01, 2022.
33. Marmarali, A. B., (2003), *Dimensional and Physical Properties of Cotton/Spandex Single Jersey Fabrics*, Textile Research Journal, 73(1), 11–14.
34. Uçar, N., Karakaş, H., Şen, S., (2007), *Physical and comfort properties of the hoisery knit product containing intermingled nylon elastomeric yarn*, Fibers and Polymers, 8(5), 558–563.
35. ASTM International, (2019), *D1777 - 96 Standard Test Method for Thickness of Textile Materials*, ASTM International, https://www.astm.org/Standards/D1777.htm, accessed Aug. 01, 2022.
36. BS EN 12127:1998, *Textiles. Fabrics. Determination of mass per unit area using small samples*, European Standards, https://www.en-standard.eu, accessed Aug. 01, 2022.
37. ASTM International, (2018), *D737-18 Standard Test Method for Air Permeability of Textile Fabrics 1*, American Society for Testing Materials,
38. ASTM International, (2019), *ASTM Standard Test Method for Breaking Force and Elongation of Textile Fabrics (Strip Method)*, https://compass.astm.org, accessed Aug. 01, 2022.
39. Khademolqorani, S., Tavanai, H., Ajalloueian, F., (2021), *Mechanical properties of silk plain-weft knitted scaffolds for bladder tissue engineering applications*, Polymers for Advanced Technologies, 32(6), 2367–2377.
40. Feng, J., (2017), *Preparation and performance control of poly(lactic acid) fiber/ polyurethane composite porous biomimetic-aligned scaffolds*, Journal of Industrial Textiles, 46(6), 1297–1318.
41. Takara, *WST-1 Cell Proliferation Assay Kit*, https://www.takara.co.kr/file/manual/pdf/MK400_v.0305.pdf, accessed Nov. 19, 2022.
42. Haroglu, D., (2021), *Development of a three dimensional (3D) knitted scaffold for myocardial tissue engineering. Part I: mechanical performance of the knitted structures*, The Journal of The Textile Institute, 113(5), 882-894.
43. Hebbar, R. S., Isloor, A. M., Ismail, A. F., (2017), *Contact Angle Measurements*, In Membrane Characterization (pp. 219–255), Elsevier Inc., Netherlands.
44. Dhania, S., Bernela, M., Rani, R., Parsad, M., Grewal, S., Kumari, S., Thakur, R., (2022), *Scaffolds the backbone of tissue engineering: Advancements in use of polyhydroxyalkanoates (PHA)*, International Journal of Biological Macromolecules, 208, 243–259.
45. Zhang, Y., Mu, W., Zhang, Y., He, X., Wang, Y., Ma, H., Zhu, T., Li, A., Hou, Q., Yang, W., Ding, Y., Ramakrishna, S., Li, H., (2022), *Recent Advances in Cardiac Patches: Materials, Preparations, and Properties*, ACS Biomaterials Science and Engineering, 8(9), 3659–3675.
46. McGregor, W. J., Tanner, K. E., Bonfield, W., Bonner, M. J., Saunders, L. S., Ward, I. M., (2000), *Fatigue properties of isotropic and hydrostatically extruded HAPEXTM*, Journal of Materials Science Letters, 19(20), 1787–1788.
47. Velayudhan, S., Martin, D., Cooper-White, J., (2009), *Evaluation of dynamic creep properties of surgical mesh prostheses—Uniaxial fatigue*, Journal of Biomedical Materials Research Part B: Applied Biomaterials, 91B(1), 287–296.
48. Siu, P. M., Wang, Y., Alway, S. E., (2009), *Apoptotic signaling induced by H2O2-mediated oxidative stress in differentiated C2C12 myotubes*, Life Sciences, 84(13-14), 468–481.
49. Jenkins, T. L., Little, D., (2019), *Synthetic scaffolds for musculoskeletal tissue engineering: cellular responses to fiber parameters*, npj Regenerative Medicine, 4(15).
50. Idaszek, J., Kijenska, E., Lojkowski, m., Swieszkowski, W., (2016), *How important are scaffolds and their surface properties in regenerative medicine*, Applied Surface Science, 388, 762–774.
51. Christopherson, G. T., Song, H., Mao, H.-Q., (2009), *The influence of fiber diameter of electrospun substrates on neural stem cell differentiation and proliferation*, Biomaterials, 30(4), 556–564.